remote sensing

MDPI

Article

Accounting for 10 m Resolution Mapping for Above-Ground Biomass of Urban Trees in C40 Cities Across Eurasia Continent

Ge Yan [1,2,3], Zhifang Shi [1,2,3], Gaomin Lian [1,2,3], Kailong Cui [1,2,3,4], Nan Li [5], Ying Luo [6], Shuyuan Zhou [7], Mengmeng Cao [1,2,3,*] and Yaoping Cui [1,2,3]

1 State Key Laboratory of Spatial Datum, Henan University, Zhengzhou 450046, China; yangeer@henu.edu.cn (G.Y.); shizhifang@henu.edu.cn (Z.S.); gaomin@henu.edu.cn (G.L.); cui@henu.edu.cn (K.C.); cuiyp@lreis.ac.cn (Y.C.)
2 Faculty of Geographical Science and Engineering, College of Geographical Sciences, Henan University, Zhengzhou 450046, China
3 Key Laboratory of Geospatial Technology for the Middle and Lower Yellow River Regions, Ministry of Education, Henan University, Kaifeng 475004, China
4 The State Key Laboratory of Information Engineering in Surveying Mapping and Remote Sensing, Wuhan University, Wuhan 430079, China
5 School of Geography and Tourism, Zhengzhou Normal University, Zhengzhou 450004, China; linan0716@henu.edu.cn
6 School of Tourism and Exhibition, Henan University of Economics and Law, Zhengzhou 450004, China; ly_075@163.com
7 Xun County Bureau of Natural Resources, Hebi 458000, China; 13783000572@163.com
* Correspondence: mmengcao@henu.edu.cn

Highlights

What are the main findings?

- This study advanced cross-city AGB mapping of urban trees to 10 m resolution.
- The AGB estimates exhibited high consistency with existing single-city C40 studies.

What are the implications of the main findings?

- Quality control markedly enhanced the random forest's fit and predictive accuracy.
- The high-accuracy inversion method developed in this study exhibited strong applicability across diverse cities.

Abstract

High-resolution above-ground biomass (AGB) data play a critical role in advancing low-carbon development strategies across cities. However, research on urban trees' AGB largely relies on high-accuracy field measurements, which limits the feasibility of conducting cross-regional studies. In contrast, existing remote-sensing-based AGB products provide extensive coverage while lacking the spatial resolution required for precise city-scale analysis. To address the dilemma of achieving both high spatial resolution and broad coverage, this study integrated 149 feature variables derived from multi-source datasets and implemented quality-control procedures to select high-quality samples from two globally representative AGB products (GEDI AGB and CCI AGB). This strategy substantially improved the performance of the random forest model and generated 10 m resolution urban trees' AGB maps for 51 C40 cities across Eurasia continent. The results indicate that: (1) after applying quality control to the target variables, the mean R^2 of ten-fold cross validation improved from 0.37 to 0.75, and the MAE decreased substantially from 47.02 Mg/ha to 17.48 Mg/ha; (2) by enhancing the spatial resolution of AGB maps to 10 m, the resulting products exhibit superior spatial detail, better capture local variations, and maintain greater spatial continuity compared with the CCI AGB and GEDI AGB datasets; (3) the mean AGB density

check for updates

Academic Editors: Dong Liu, Jiakui Tang and Qing Zhang

Received: 30 October 2025
Revised: 27 November 2025
Accepted: 28 November 2025
Published: 30 November 2025

Citation: Yan, G.; Shi, Z.; Lian, G.; Cui, K.; Li, N.; Luo, Y.; Zhou, S.; Cao, M.; Cui, Y. Accounting for 10 m Resolution Mapping for Above-Ground Biomass of Urban Trees in C40 Cities Across Eurasia Continent. *Remote Sens.* **2025**, *17*, 3898. https://doi.org/10.3390/rs17233898

Copyright: © 2025 by the authors. Licensee MDPI, Basel, Switzerland. This article is an open access article distributed under the terms and conditions of the Creative Commons Attribution (CC BY) license (https://creativecommons.org/licenses/by/4.0/).

across the Eurasian continent was 39.44 Mg/ha, with total urban tree s' AGB reaching 83.83 × 10^6 t. Comparison with previous single-city C40 studies shows that our estimated AGB density and total AGB closely align with previously reported values. The above data implies that cities carry an undeniable amount of carbon storage, both in terms of carbon density and total amount. This study provides a robust foundation for accurately assessing the potential of urban carbon sinks and optimizing the path to achieving carbon neutrality.

Keywords: C40 cities; above-ground biomass; random forest; urban trees; remote sensing mapping

1. Introduction

Cities, being primary contributors to greenhouse gas emissions and hotspots of climate vulnerability, are increasingly recognized as critical fronts in international climate governance [1,2]. The C40 Cities Climate Leadership Group (C40) in Eurasia continent encompasses nearly fifty key global cities, with the goal of advancing emission reduction efforts, strengthening climate resilience, and accelerating the transition to low-carbon urban development through inter-city collaboration [3,4]. In this context, urban trees—key elements of urban ecosystems—are widely regarded by C40 members as vital natural solutions, owing to their multifunctional roles in carbon sequestration, climate regulation, and biodiversity protection [5–7]. AGB serves as a fundamental metric for quantifying the carbon sequestration capacity of urban trees and evaluating their contribution to the urban carbon cycle [8,9]. Nevertheless, due to limitations in basic data availability and the precision of current AGB products, accurately estimating AGB at the scale of urban trees and achieving urban carbon neutrality continue to pose substantial challenges [10].

Currently, AGB data for individual cities are usually obtained through conventional field measurements, offering high-accuracy estimates at local scales [11]. However, field measurements are labor-intensive and challenging to scale across large regions, which constrains cross-city comparisons and comprehensive analyses [12,13]. In contrast, leveraging multi-source remote sensing data has emerged as a critical approach to surmounting the limitations of large-scale urban trees' AGB assessment [14]. Nevertheless, in the context of highly heterogeneous and complex urban landscapes, the suitability of different remote sensing datasets is influenced by multiple limiting factors [15,16]. Optical remote sensing imagery is commonly affected by clouds and mixed pixels; SAR, a type of microwave remote sensing, experiences signal distortion in densely built urban areas due to multiple reflections; and LiDAR, capable of precisely capturing vegetation's three-dimensional structure, is constrained by limited coverage and high acquisition costs [17–21]. In terms of data resolution, low-resolution data hinder the ability to capture the heterogeneity of trees within urban areas. Although several medium- and high-resolution AGB datasets are available, many lack the consistent spatial coverage necessary for cross-regional analyses [22,23]. In recent years, spaceborne LiDAR has generated AGB estimates (e.g., GEDI AGB), helping to address the lack of large-scale AGB datasets. Additionally, high-resolution AGB products derived from multi-source remote sensing fusion (e.g., CCI AGB) provide reference benchmarks for AGB estimation at regional and global scales [24]. These two datasets offer critical and complementary support for estimating urban AGB at fine scales across large geographic regions.

AGB estimation using remote sensing data generally depends on either parametric or non-parametric modeling approaches [25]. Parametric models are simple and easy to implement but sensitive to outliers such as parameters of the allometric growth equation

for the same forest in different growth environments, and often ignore variable correlations; non-parametric models capture nonlinear relationships between predictors and field measurements, demonstrating superior generalization in large-scale AGB estimation [26,27]. Typical non-parametric approaches include k-nearest neighbors (k-NN), support vector machines (SVM), and random forest (RF) models [28]. Notably, the random forest model, with its robust ability to model nonlinear relationships and select relevant features, has demonstrated high reliability in estimating biomass in forests with complex structures [29,30]. However, the accuracy of model predictions fundamentally depends on the reliability of the target variable [31]. At present, GEDI AGB data do not provide continuous coverage for C40 cities across Eurasia continent, and the accuracy of the derived 1 km raster products relies on the original footprint data. Meanwhile, the 100 m spatial resolution of CCI AGB products is still inadequate for fine AGB mapping of urban trees [32,33]. Furthermore, discrepancies between the two datasets at identical locations, coupled with their inherent quality constraints, further complicate accurate AGB estimation. Consequently, we developed quality-control procedures to select reliable training samples from both the GEDI AGB and CCI AGB products. These high-quality samples then served as robust target variables for the random forest model, enabling high-precision inversion of urban trees' AGB.

In this study, C40 cities across the Eurasian continent were selected as the study area. Multidimensional indicators—including spectral, textural, and vegetation indices derived from Sentinel-2A/B imagery—were used as feature variables. High-quality samples were selected from the GEDI AGB and CCI AGB datasets through quality-control procedures and subsequently served as target variables for training the random forest model. Model performance before and after quality control was assessed using ten-fold cross validation, and high-accuracy urban-tree's AGB maps were ultimately generated for 51 C40 cities. The findings can advance the focus of AGB research toward the urban scale and offer a foundation for assessing the ecological and carbon sequestration functions of urban trees.

2. Data and Methods

2.1. Study Area

The C40 is an international coalition of 96 megacities, each with a population of over three million [34]. About 53% of C40 cities are situated across the Eurasian continent, predominantly clustered within 100 km of the coastline in land–sea transitional zones, forming major coastal urban agglomerations centered on the Pacific Rim and North Atlantic regions (Figure 1). The region spans diverse landforms—from low-lying coastal plains to high mountain gorges—and encompasses a wide climatic gradient from tropical rainforests to tundra (Table S1) [35,36]. Cities in this region, characterized by varied urbanization levels, broad climatic diversity, and availability of high-quality remote sensing datasets, offer ideal natural conditions for large-scale evaluation of urban trees' AGB.

2.2. Data

2.2.1. Remote Sensing Satellite Imagery

This study employed 10 m Sentinel-2A/B Level-2A imagery accessed via the Google Earth Engine (GEE) platform to extract spectral and textural features and compute vegetation indices for urban trees analysis. Sentinel-2 images with cloud cover below 5% acquired between April and November 2020 were prioritized for annual compositing. When imagery meeting these conditions was unavailable, the cloud cover threshold was relaxed to 10%, and the nearest available images to the base year (2018–2022) were used as replacements (Table S2).

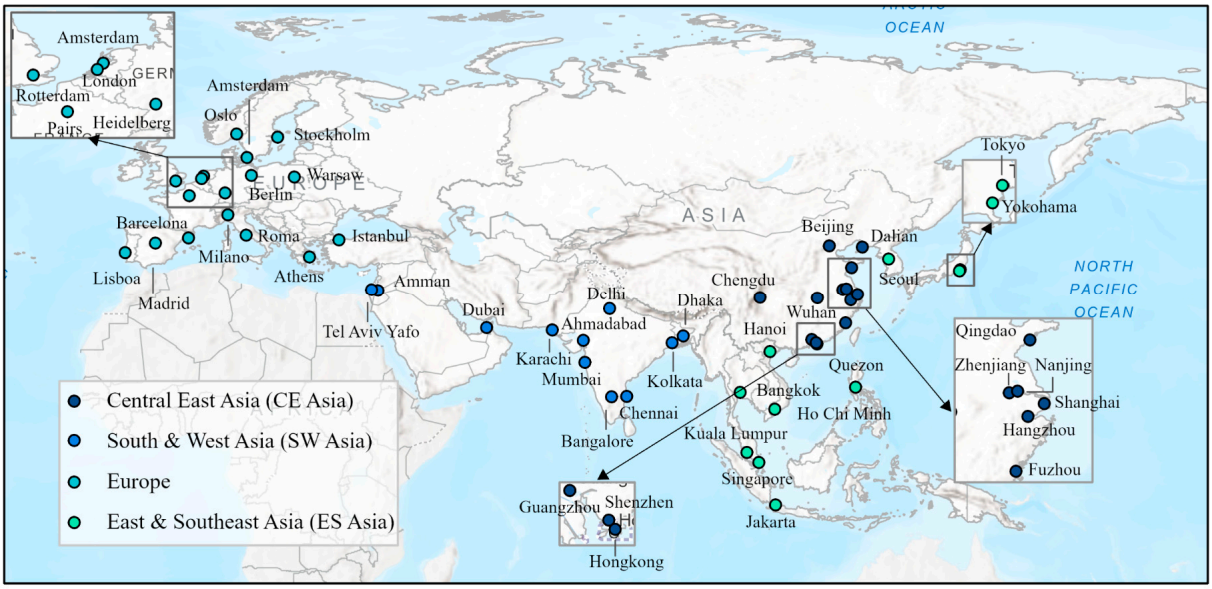


Figure 1. Overview of C40 cities across Eurasia continent.

2.2.2. AGB Data Products

In this study, two global AGB datasets were employed: the 25 m resolution Level 4 AGB product from the Global Ecosystem Dynamics Investigation (GEDI AGB, https://daac.ornl.gov/cgi-bin/dataset_lister.pl?p=40 (accessed on 25 September 2024)) and the 100 m resolution AGB estimates from the European Space Agency Climate Change Initiative (CCI AGB, https://climate.esa.int/en/projects/biomass/data/ (accessed on 2 October 2024)). The GEDI AGB provides detailed information on forest vertical structure with high spatial precision. The product is processed across four levels, with L3 interpolating L2 footprint data into 1 km grids, and L4 converting L2 vertical structure parameters into above-ground biomass density estimates, providing 25 m resolution L4A footprint-level data. The CCI AGB dataset covers all forest ecosystem types and exhibits high estimation accuracy in high-biomass regions, providing annual products for 2010 and for the period 2017–2021 [37,38]. The GEDI_AGBD dataset employed in this study spans April to November 2020, while the CCI AGB dataset corresponds to 2020, ensuring temporal consistency with the Sentinel-2A/B imagery acquisition period. After applying quality control procedures to both datasets, high-quality samples within the C40 cities were extracted and used to construct the target variables for urban trees' AGB inversion.

2.2.3. AGB Data for Urban Trees

According to the ESA WorldCover 2020 global 10 m resolution land cover product (https://livingatlas.arcgis.com/landcover/ (accessed on 15 September 2024)), the "trees" category is defined as tall, densely canopied vegetation exceeding 4.5 m in height, including natural forests, plantations, and mangroves [39]. In addition, the UNFAO-FRA land classification framework defines biophysical thresholds for canopy cover (FVC), height (H), and area (S) to differentiate tree categories within urban environments [40]. As this study targets trees outside forests (TOF) and emphasizes individual-tree vegetation, the UNFAO-FRA Set-2 biophysical thresholds were simplified to delineate TOF and derive the urban-tree class used in this study (Method S1). Based on this, pixels representing urban trees and their corresponding AGB values were extracted to ensure that the selected target variables correspond specifically to urban trees rather than other land-cover types.

2.3. Methods

2.3.1. Random Forest Model

The random forest model trains multiple decision trees on randomly selected subsets of features and samples, aggregating their predictions via averaging or voting to reduce overfitting and enhance model generalization [41,42]. It learns nonlinear predictor–response relationships at coarse resolutions and then transfers these learned relationships to finer-resolution predictors [43]. To prevent overfitting and improve generalization, a grid search was employed to optimize random forest hyperparameters in this study (Table S3). This study first resampled the Sentinel-2A/B–derived variables from 10 m to match the original resolutions of the GEDI AGB (25 m) and CCI AGB (100 m) products. Using the random forest model, this study independently modeled the relationships between the resampled Sentinel-2A/B variables and each AGB product. The trained models were subsequently applied to the original 10 m Sentinel-2A/B variables to generate refined AGB predictions at a 10 m resolution (Figure 2).

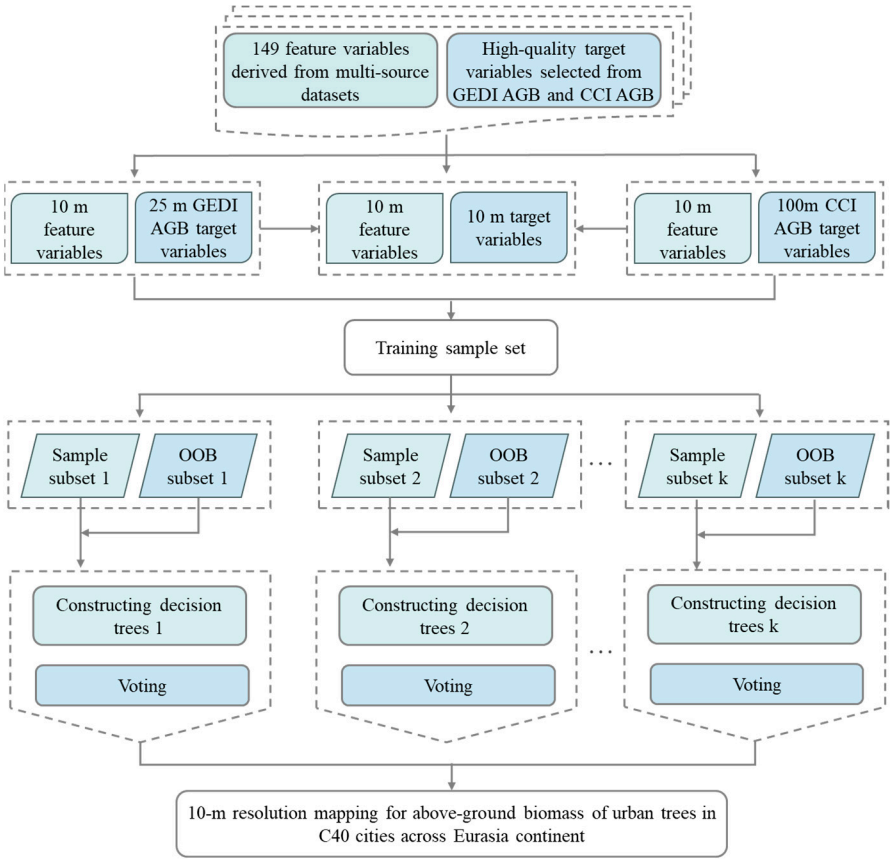


Figure 2. Flowchart of the random forest model.

2.3.2. Multidimensional Feature Variables Extraction

Spectral-derived variables such as vegetation indices, band reflectance, and band ratios serve as key predictors for estimating tree AGB using remote sensing. However, their performance can be limited under complex environmental conditions due to spectral saturation, which hinders accurate predictions [44]. As derivatives of remote sensing imagery, texture information can reveal spatial arrangement patterns and morphological differences of features from micro- to macro-scales and has increasingly become a key auxiliary variable for AGB estimation [45]. Using Sentinel-2A/B imagery on the GEE platform, this study calculated 46 vegetation indices reported in the literature (Table S4) [46–76]. and Eight categories of GLCM texture features were also extracted from

10 spectral bands as well as a fused grayscale band (Table S5). Moreover, previous studies have shown that incorporating forest canopy height into optical remote sensing imagery for biomass estimation can significantly improve AGB prediction accuracy [49]. Therefore, the fused tree canopy height data (TCH) with 10 m resolution independently constructed by our team were used as an auxiliary feature variable (Method S2). By integrating the 13 original Sentinel-2 spectral bands, the fused grayscale band, a feature sample library containing 149 variables was ultimately established (Table S6).

To minimize the introduction of unnecessary noise from high-dimensional predictors, this study applied the Boruta feature-selection algorithm to the initial set of 149 variables. Based on the mean importance scores derived from 30 iterations, 32 feature variables were retained as input variables for the random forest model. Among them, B9, B1, and B10 from the original Sentinel-2 imagery ranked as the top three most important features (Table 1).

Table 1. Feature variables input to the random forest model.

Variable Types	Variable Components	Number
Vegetation Indices	MDNVI, AGRI, WDRVI, NG	4
Sentinel-2 raw bands	B1, B2, B9, B10, B11, B12	6
Texture features	B6_IDM, B8_IDM, B2_VAR, B11_VAR, B12_VAR, B8_DISS, B11_DISS, B12_DISS, B2_CON, B8_CON, B12_CON, B11_CON, B2_SAVG, B3_SAVG, B4_SAVG, B5_SAVG, B7_SAVG, B8A_SAVG, B11_SAVG, B12_SAVG, Gray_SAVG	21
Other	TCH	1
	Total	32

2.3.3. Quality Control Procedures Construction

Given that AGB datasets containing systematic bias can distort the statistical relationships between predictor and target variables, which may amplify prediction errors and increase sensitivity to local noise [77,78]. In addition, mixed-pixel effects merge signals from multiple land-cover components and weaken the generalization capacity of machine-learning models [79]. To address these issues, this study developed quality-control procedures to extract high-quality AGB samples from the GEDI AGB and CCI AGB products to support large-scale AGB mapping (Figure 3):

(1) Land Cover Data Masking: Using the "trees" category from the ESA WorldCover 2020 global 10 m resolution land cover product, GEDI AGB and CCI AGB data were masked. CCI AGB values corresponding to the masked GEDI footprint points were then extracted.

(2) Quality Control Layer Constraints: Based on the GEE platform, core parameters from the GEDI L4A dataset—including agbd, agbd_se, l4_quality_flag, and degrade_flag inherent in the quality data—were extracted. Target variables with a relative standard error (RSE = agbd_se/agbd) exceeding 30% were first removed, and outliers flagged with l4_quality_flag = 0 were subsequently excluded.

(3) Training Data Cleaning: Outliers in the target variables were identified and removed based on the interquartile range (IQR) calculated using the boxplot method [80]. At the same time, all 46 vegetation index features were standardized to remove the effect of scale differences on model performance.

(4) Training Data Mutual Validation: Under the assumption that AGB estimates follow a normal distribution, the values from each dataset are expected to fluctuate around the true biomass at a given pixel [81]. To systematically identify samples with relatively high

consistency between the two datasets, following the above steps, we treated each dataset in turn as the reference variable and calculated the ratio between the two target variables at each pixel. When this ratio exceeded 90%—indicating that the deviation between the two datasets was within 10%—the corresponding denominator variable was identified as a high-quality sample.

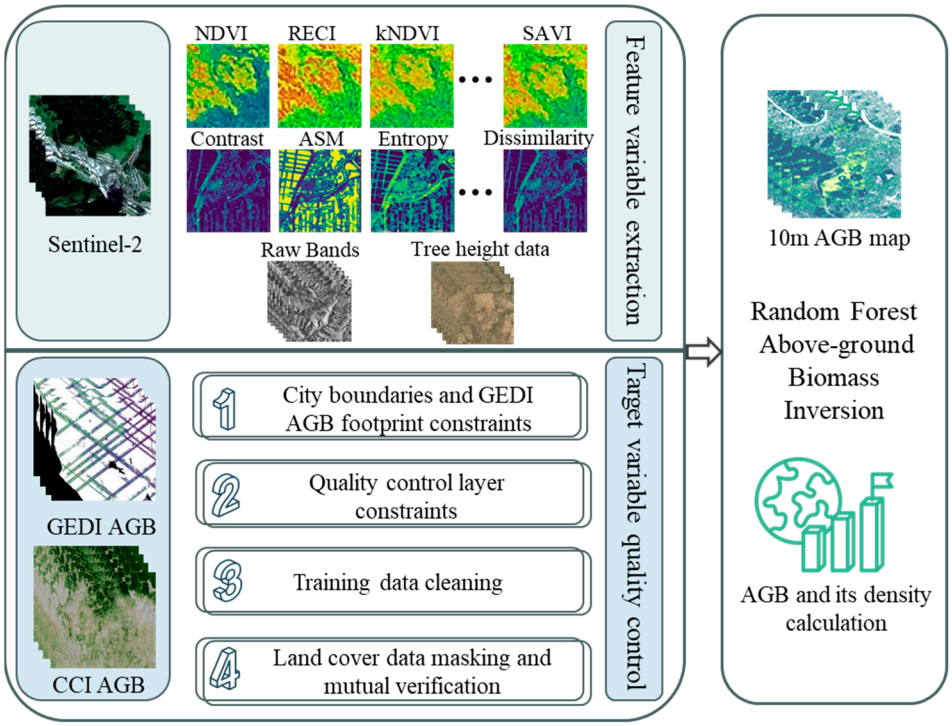


Figure 3. Research flowchart.

2.3.4. Model Accuracy Evaluation

Ten-fold cross validation partitions the original dataset into 10 subsets, iteratively using nine subsets for training and one subset for testing [82]. This procedure is repeated until each subset has served as the test set, and the mean of the ten results is taken as the overall evaluation of the model's performance [83]. In this study, ten-fold cross validation was employed to assess the predictive performance of the model, with the coefficient of determination (R^2) and mean absolute error (MAE) used as the primary accuracy metrics.

3. Results

3.1. Comparison of Target Variable Quality Control Results

Applying quality control procedures to the CCI AGB and GEDI AGB datasets substantially enhanced the performance of the random forest model for AGB inversion. To assess the improvement in model accuracy following quality control, two sets of target variable datasets were created. First, the preprocessed GEDI AGB and CCI AGB datasets were clipped to the boundaries of the C40 cities, and CCI AGB values were extracted at the corresponding GEDI footprint locations; these datasets were then used independently as target variables to construct the initial training datasets. Second, the high-quality samples obtained from the GEDI and CCI AGB datasets through quality-control procedures were used to form the quality-controlled training datasets. When using only the initial training datasets, the ten-fold cross validation results showed that the model achieved R^2 = 0.37 and MAE = 47.02 Mg/ha when using CCI AGB as the target variable, and R^2 = 0.21 and MAE = 40.76 Mg/ha when using GEDI AGB as the target variable (Figure 4). The model accuracy was notably below the baseline level (R^2 = 0.68), with persistently high prediction

errors, suggesting that directly using the raw target variables cannot yield satisfactory estimation accuracy. When using the quality-controlled training datasets, ten-fold cross validation revealed that when CCI AGB data were used as the target variable, the R^2 of the random forest model markedly increased to 0.75 and the MAE decreased to 17.48 Mg/ha; with GEDI AGB data as the target variable, R^2 improved to 0.28 and MAE declined to 30.14 Mg/ha (Figure 5). The above results indicate that the high-quality samples selected through quality control substantially enhanced the fitting accuracy and predictive stability of the random forest model, offering a robust data foundation for the high-precision mapping of urban trees' AGB in subsequent analyses.

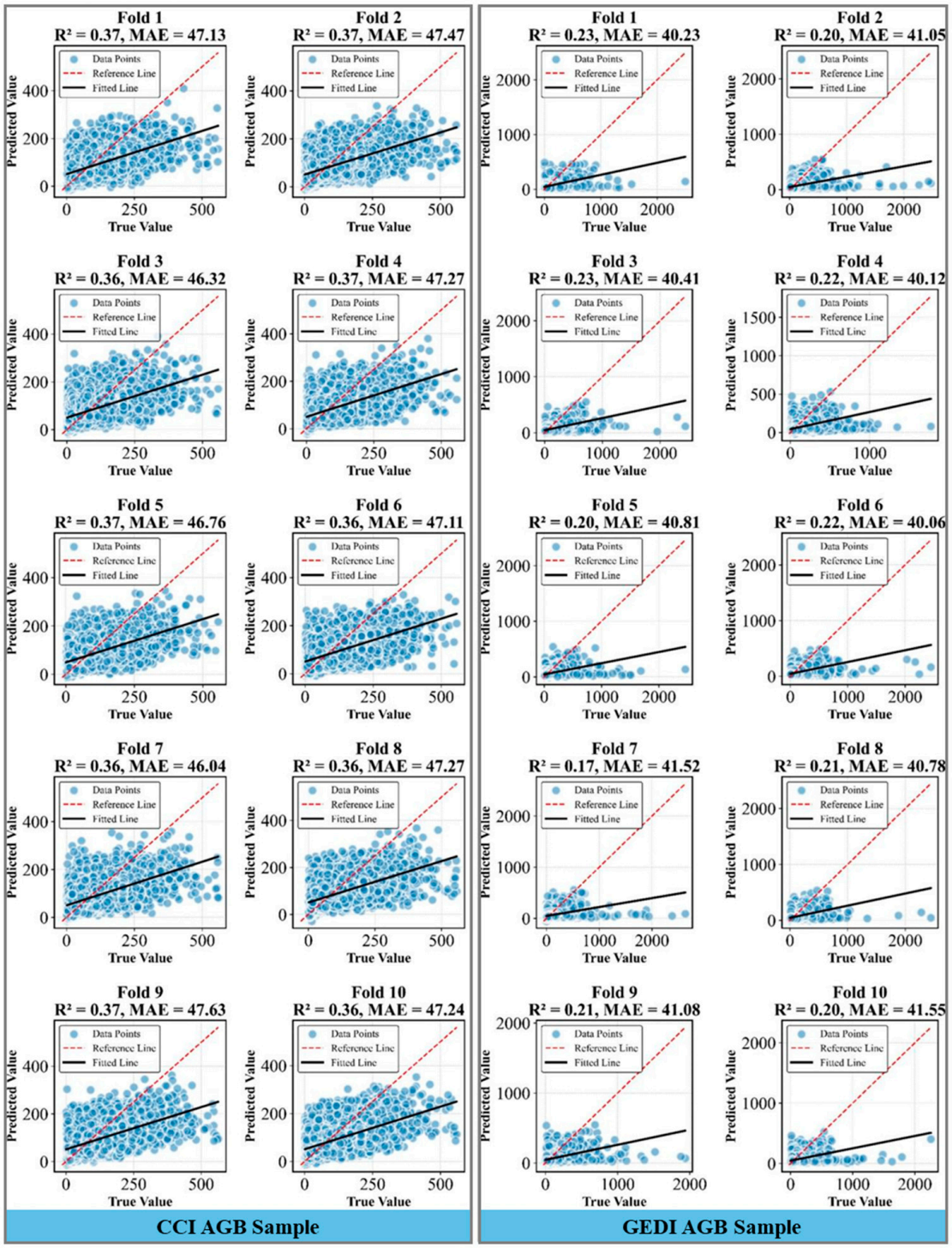


Figure 4. Ten-fold cross validation of simulation results before quality control.

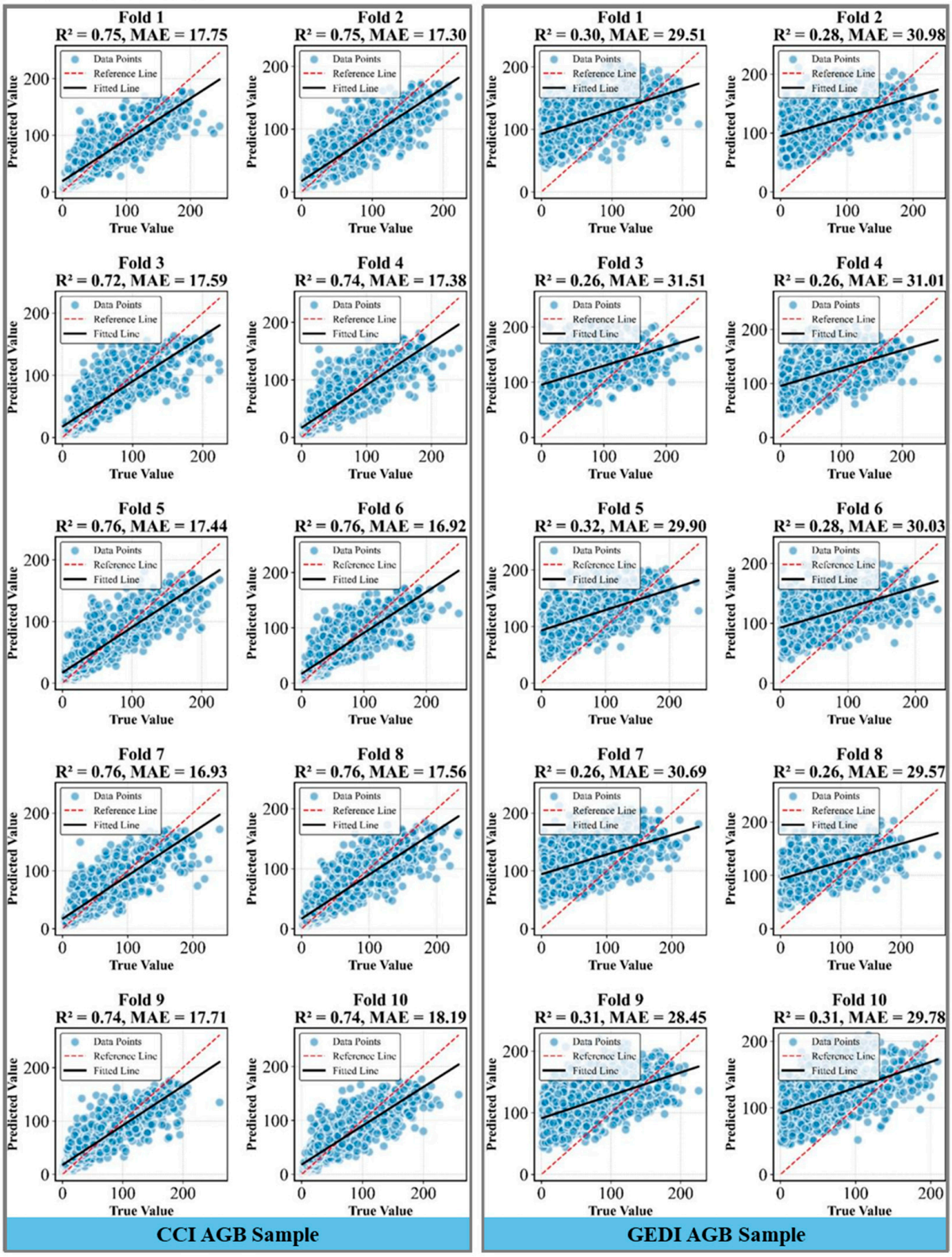


Figure 5. Ten-fold cross validation of simulation results after quality control.

3.2. Assessment of Urban Trees' AGB Density and Total AGB

The mean AGB density of urban trees in C40 cities across the Eurasian continent reached 39.44 Mg/ha, with substantial regional variations observed among cities (Figure 6a). In the Central East Asia, the average AGB density is 40.65 Mg/ha, ranging from a minimum of 29.16 Mg/ha in Dalian to a maximum of 64.63 Mg/ha in Shenzhen. Among all regions,

the South and West Asia exhibited the lowest average AGB density, measuring 31.98 Mg/ha. At the urban scale, Mumbai exhibited the highest AGB density at 40.97 Mg/ha, while Bangalore recorded just 25.51 Mg/ha, the lowest value both within the region and across the entire study area. In Europe, the average AGB density was 40.77 Mg/ha, with Madrid recording the lowest value at 26.28 Mg/ha and Stockholm the highest at 59.93 Mg/ha. In East and Southeast Asia, the average AGB density reached 43.81 Mg/ha, representing the highest value among the four Eurasian regions. Within the region, Ho Chi Minh recorded the lowest AGB density at 33.78 Mg/ha, while Yokohama exhibited the highest at 65.74 Mg/ha, making it the densest city among all C40 cities. Analysis of the spatial distribution of AGB density in cities with extreme values shows that Yokohama's high-density areas form multiple clusters, low-density areas are relatively sparse, and the city exhibits a generally high overall density (Figure 6b). By comparison, Bangalore's city center displayed markedly low AGB density, with few high-density zones and a clear pattern of clustered low-density areas (Figure 6c).

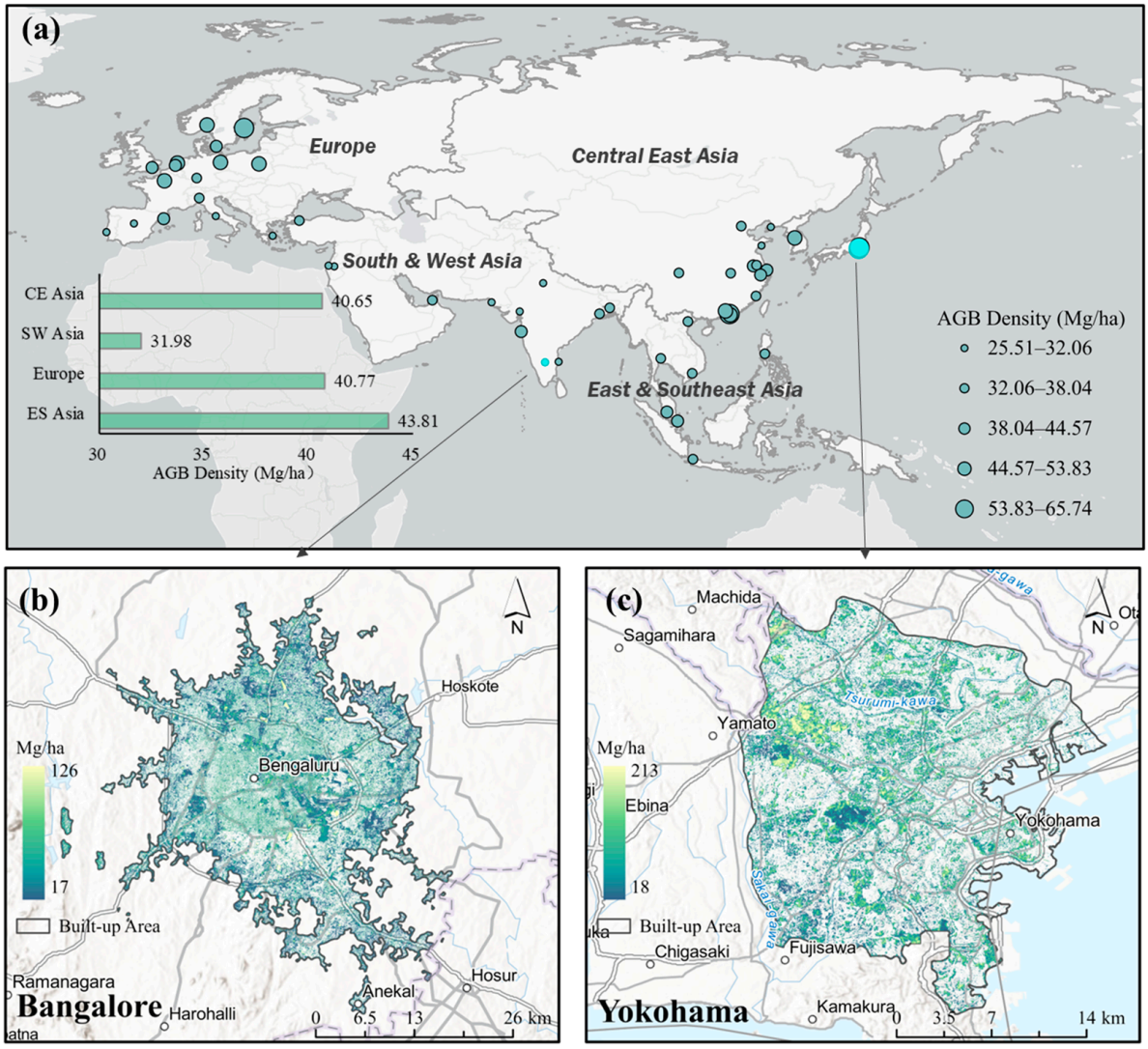


Figure 6. Results of urban trees' AGB density in the study area. (**a**) AGB density distribution along with the regional mean values; (**b**) spatial distribution of AGB in Bangalore, the city with the lowest density; (**c**) spatial distribution of AGB in Yokohama, the city with the highest density.

The cumulative AGB of C40 cities on the Eurasian continent reached 83.83 $\times$ 10^6 t, with inter-city differences as high as 8.26 $\times$ 10^6 t (Figure 7). Across a total area of

4117.79 km^2, the 11 C40 cities in the South and West Asia collectively contributed 5.23 × 10^6 t of AGB, representing the lowest total among all regions. In this region, Dubai exhibits the lowest total AGB of 0.09 × 10^6 t, whereas Delhi reaches the highest value of 1.37 × 10^6 t. With a comparable number of cities (10), East and Southeast Asia accumulated a total AGB of 8.87 × 10^6 t. Within the region, Quezon recorded the lowest AGB at 0.21 ×10^6 t, while Bangkok exhibited the highest at 1.75 × 10^6 t. Despite including only 13 C40 cities, Central East Asia accumulated a total AGB of 48.70 × 10^6 t, making it the highest among the four regions. Within this region, Beijing exhibited the highest AGB at 8.42 × 10^6 t among all C40 cities in Eurasia continent, whereas Hong Kong's AGB was merely 0.59 × 10^6 t. Europe hosts the most C40 cities (17 in total), accumulated a total of 21.04 × 10^6 t of AGB across roughly 10,115.97 km^2. Heidelberg registered the lowest total AGB at 0.06 × 10^6 t both regionally and among all cities in the study, whereas London exhibited the highest AGB within the region at 3.83 × 10^6 t.

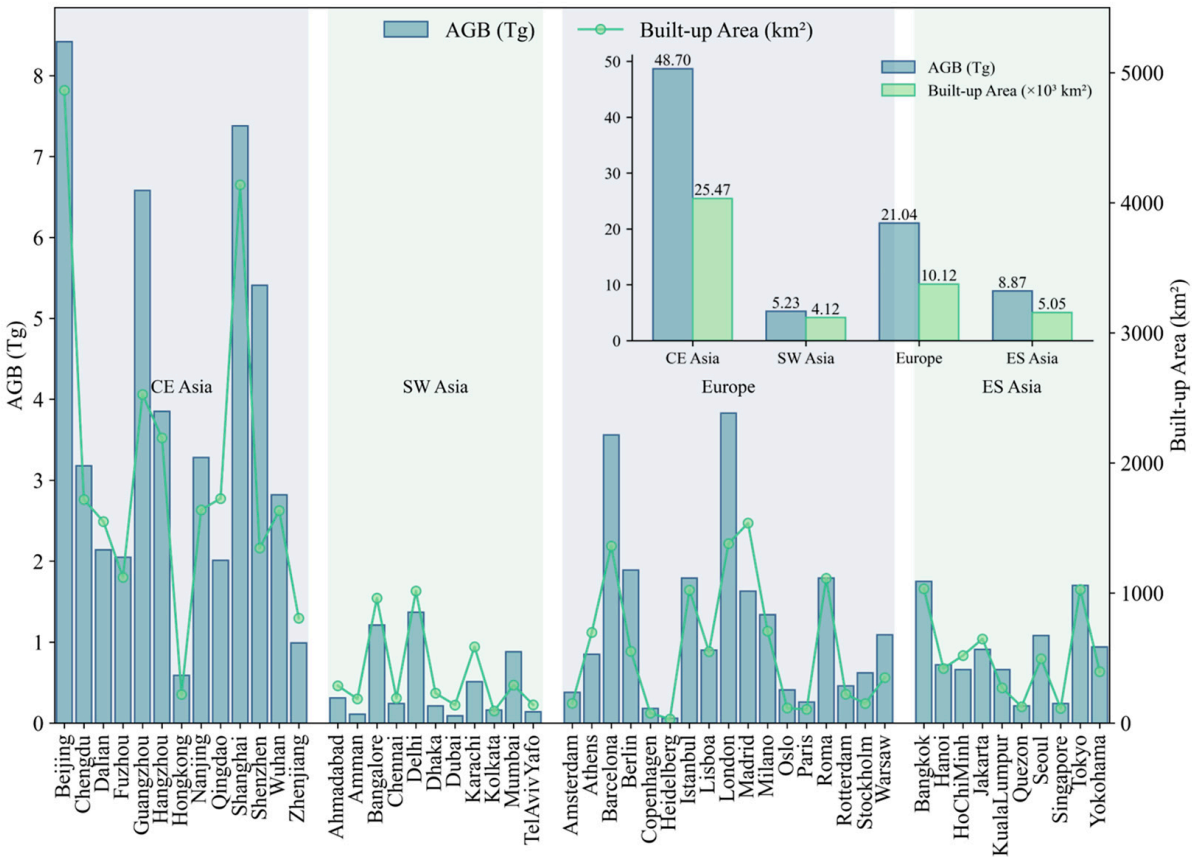


Figure 7. Results of urban trees' AGB in the study area.

3.3. Comparison of Spatial Mapping Details for Urban Trees' AGB

At the scale of individual cities, the AGB maps produced in this study demonstrated superior spatial detail, enhanced detection of local variations, and greater spatial continuity compared with CCI AGB and GEDI AGB datasets (Figure 8). The distribution of urban trees varies markedly due to the combined effects of geographic conditions and urban development planning, consequently shaping the AGB of individual cities [84,85]. To systematically evaluate the applicability of the AGB mapping results across different urban environments, representative cities from various climate zones were selected for comparative analysis against CCI AGB and GEDI AGB datasets. In tropical cities such as Bangkok and Kuala Lumpur, dense urban structures lead to trees being scattered or forming small patches. Under these conditions, CCI AGB captures only a limited number of pixels,

while GEDI AGB lacks spatial continuity. In comparison, the AGB mapping developed in this study enables complete extraction of green spaces and accurately identify scattered trees in densely built-up areas. In the subtropical cities of Athens and Tokyo, which feature complex internal ecological landscapes, CCI AGB showed slightly better performance in Tokyo but provided limited detail; GEDI AGB was affected by pixel gaps and coarse resolution, while the AGB mapping in this study effectively captured subtle variations in tree density. In cities with extensive suburban tree coverage, including Beijing and London, the two datasets showed limitations in delineating tree distributions along rivers and major roads and in representing internal density variations. In contrast, the AGB mapping developed in this study enables comprehensive delineation of trees' linear distribution features while precisely capturing their internal spatial heterogeneity. Overall, the AGB mapping developed in this study achieves high accuracy in both densely urbanized areas and tree-abundant suburban zones, markedly surpassing existing AGB datasets in detailing fine-scale features and capturing spatial heterogeneity.

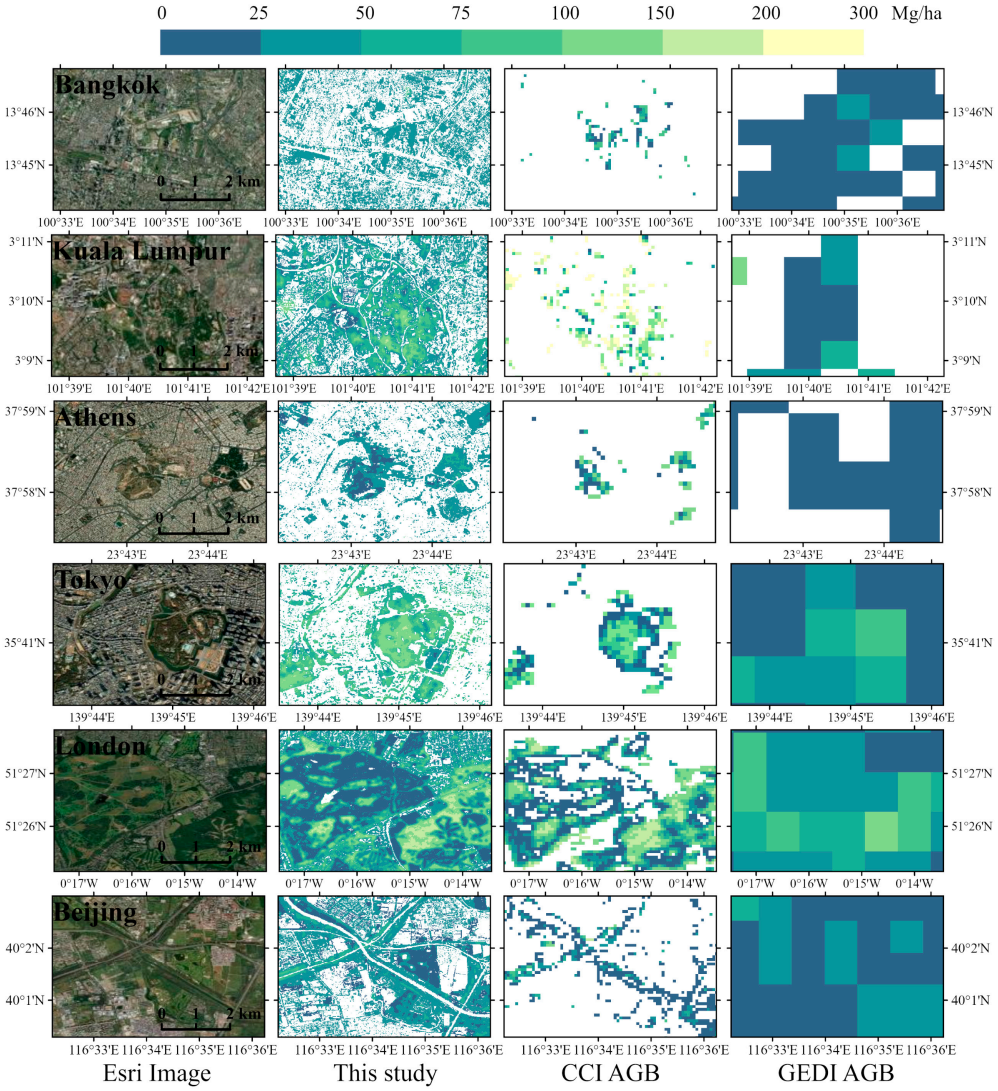


Figure 8. Comparison of AGB mapping developed in this study against CCI AGB and GEDI AGB.

4. Discussion

4.1. Comparison of AGB Estimates and Mapping Accuracy with Previous Studies

Comparative analysis with existing urban studies indicates that this study shows high consistency in both total biomass and density estimates. The results of this study

were compared with existing research data covering 12 cities, including Berlin, London, and Beijing. Given that the spatial extents of previously published AGB estimates differ substantially from the areas delineated in this study, the reported AGB values were recalculated using an area-weighted adjustment to eliminate comparison bias (Table 2). The results indicate that, in terms of AGB, this study estimated 1.15099×10^8 t for Beijing, while previous research reported 1.14777×10^8 t, with a difference of only 0.003×10^8 t [86,87]. In contrast, the AGB estimated for Chengdu in this study is 3.6969×10^6 t, while that reported in previous research is 8.3556×10^6 t, with an error of approximately 4.66×10^6 t [88]. This discrepancy is primarily attributed to the much larger spatial extent considered in the previous study (16,419 km^2) compared with this study (1150.99 km^2), which included extensive non-urban forested areas. In addition, Chennai and Nanjing were not included in the complete comparison because of data unavailability or unclear area definitions [89,90]. Regarding AGB density, the estimated value for Beijing in this study (36.81 Mg/ha) closely matches that of previous research (34.24 Mg/ha), with a relative deviation of merely 2.57 Mg/ha [91]. In contrast, Shenzhen shows a larger difference, with this study estimating 64.63 Mg/ha compared to 89.88 Mg/ha reported previously, representing a discrepancy of approximately 25.25 Mg/ha [92,93]. Some cities, such as Chengdu (36.98 Mg/ha compared with 23.42 Mg/ha) and Nanjing (40.29 Mg/ha compared with 33.84 Mg/ha), exhibited slightly larger differences, mainly due to variations in model assumptions and estimation principles between allometric equations and machine learning approaches [88,90]. The above results indicate that the multi-city AGB inversion based on remote sensing data in this study is highly consistent with measured data from individual cities. This not only validates the high-accuracy inversion capability of the method under conditions of limited ground observations, but also highlights its strong applicability across cities. Despite efforts to broaden the comparison by incorporating additional cities from multiple world regions, published studies providing city-level AGB estimates specifically for urban trees remain scarce. Consequently, the comparison set exhibits regional clustering and may not fully capture the heterogeneity of global urban environments. As more comparable city-scale AGB datasets become available, future research should incorporate a more regionally balanced set of reference studies to enable a more comprehensive assessment of methodological applicability across diverse urban contexts.

Table 2. Comparison of AGB and AGB density between this study and other C40 city studies.

	This Study			Other Studies			
City	**Area (km^2)**	**AGB (10^4 t)**	**AGB Density (Mg/ha)**	**Area (km^2)**	**Weighted AGB (10^4 t)**	**AGB Density (Mg/ha)**	**Ref.**
Beijing	4863.77	1150.99	36.81	16,410.00	1147.77	34.24	[86,87,91]
Berlin	552.35	310.45	46.65	890.00	348.39	-	[94]
Chengdu	1718.46	369.69	36.98	5662.33	835.56	23.42	[88]
Chennai	190.83	31.40	32.06	176.00	-	36.80	[89]
Hangzhou	2191.93	456.32	40.16	1766.97	277.24	34.76	[95]
London	1379.71	613.96	41.70	21.80	696.17	51.70	[12]
Nanjing	1638.10	391.77	40.29	-	271.40	33.84	[86,87,90,91]
Paris	104.92	26.08	53.83	104.92	45.88	43.73	[96]
Seoul	495.23	107.59	47.43	39.6	150.07	-	[97]
Shanghai	4136.65	842.00	41.54	688.00	-	47.80	[98]
Shenzhen	1344.70	590.55	64.63	1997.47	665.52	89.88	[88,92,93]
Singapore	112.71	24.43	39.10	-	-	32.88	[99]

To further evaluate the accuracy of the AGB products developed in this study, we searched for comparable datasets with similar spatial resolution. However, most publicly available AGB maps covering all C40 cities are of relatively coarse resolution, whereas high-resolution products are typically commercial and difficult to obtain, leaving very few datasets suitable for direct comparison. Through a literature review, we identified two published high-resolution AGB maps of Europe. The first dataset, produced by Liu et al., provides 30 m AGB maps generated from 3 m nanosatellite imagery across Europe [100]. The second dataset, produced by Jukka et al., offers a 10 m AGB map developed using species-specific Pan-European timber volume and AGB information derived from 14 National Forest Inventories comprising about 151,000 field plots [101]. Comparing the three AGB maps reveals that the Jukka map provides weaker spatial detail and coherence than both our map and the Liu map (Figure 9). In contrast to the Liu map, our map maintains strong agreement in the overall spatial patterns of urban trees' AGB. At the same time, it more accurately captures the dispersed distribution of urban trees within densely built-up areas, as well as the linear or ring-shaped patterns shaped by major roads, rivers, and terrain. Moreover, compared with the deep learning approach employed by Liu et al., the random forest model used in this study achieves relatively higher accuracy while relying on a simpler methodology.

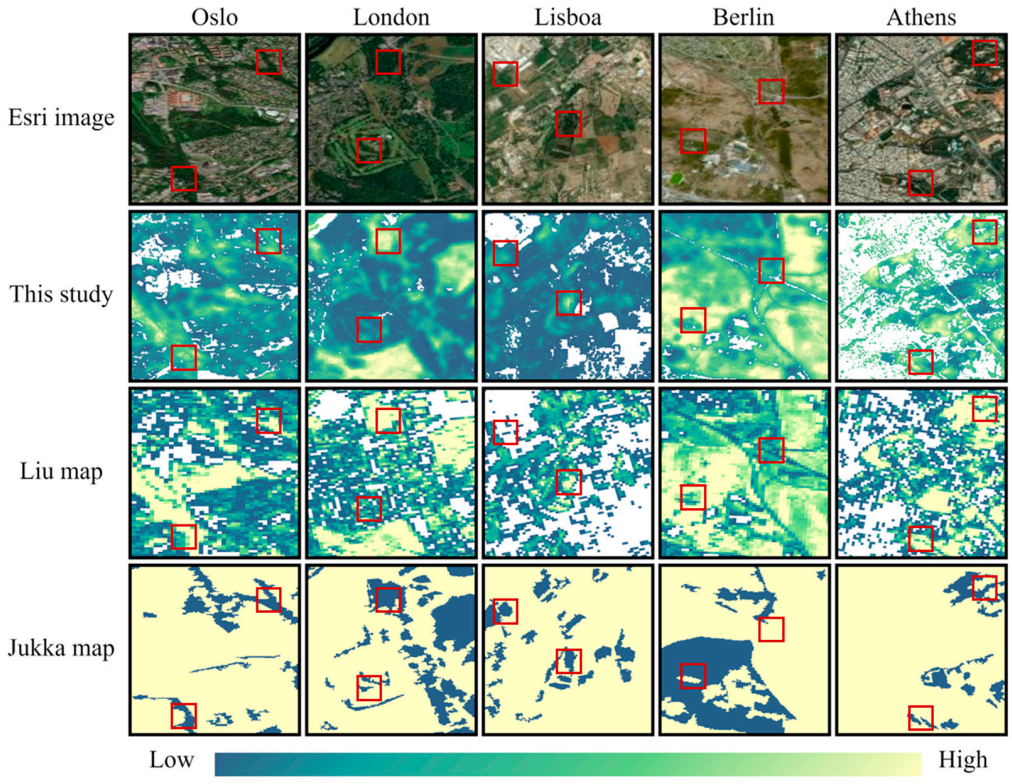


Figure 9. Comparison of the 10 m AGB maps generated in this study with other 10 m AGB maps across European cities.

4.2. The Necessity and Potential Limitations of Accurately Estimating Urban Trees' AGB

The L4-level GEDI AGB product offers 25 m resolution but is limited to footprint points and lacks continuous spatial coverage, whereas the L4A-derived raster product, with 1 km resolution, cannot meet the requirements for high-resolution AGB estimation of urban trees [96,102]. Similarly, despite the 100 m resolution of the CCI AGB dataset, smoothing effects at the local scale limit its ability to resolve fine variations in urban trees' AGB [103–105]. This study achieved 10 m–level cross-regional mapping accuracy, effectively preventing the omission of small or sparsely distributed urban trees due to scale

constraints. Moreover, the methodological framework established in this study—combining multi-source remote sensing data with rigorous quality control—exhibits strong scalability and can be extended to multiple cities, providing a solid basis for systematic comparisons of urban trees' AGB across different regions. On this basis, the total AGB of urban trees across the study area was estimated at 83.83 $\times$ 10^6 t, markedly surpassing Canada's national urban forest AGB (67.96 $\times$ 10^6 t) and exceeding Albania's total national AGB (72.97 $\times$ 10^6 t) [106,107]. This suggests that urban trees, as a critical element of regional carbon sinks, play a pivotal role in boosting carbon storage and facilitating progress toward regional carbon neutrality. Despite urbanization encroaching on farmland and some forested areas, forests maintain substantially higher carbon density per unit area compared with farmland, grassland, water bodies, and unused land, with urban trees alone comprising approximately 97% of total urban AGB [108,109]. This not only indicates that optimizing urban spatial layout and increasing forest cover can significantly enhance the carbon storage capacity of future urban ecosystems, but also further suggests that incorporating urban trees into carbon accounting frameworks helps improve the scientific rigor and accuracy of urban carbon stock assessments.

Currently, field-based measurements of urban tree AGB in C40 cities are relatively scarce [23]. Large-scale estimation largely relies on globally available AGB datasets-such as GEDI AGB and CCI AGB-which provide extensive spatial coverage and are suitable for machine-learning applications. By applying quality control to GEDI AGB and CCI AGB datasets, this study established a highly reliable sample set, thereby partially mitigating the constraints imposed by the limited availability of large-scale field measurements data. Nevertheless, incorporating accurate field measurements remains indispensable for further enhancing the reliability of the results generated in this study. At the same time, thoroughly investigating how uncertainties in input variables propagate through the random forest model represents an important avenue for methodological improvement in future research. In addition, current research frequently relies on vegetation-sensitive optical remote sensing imagery for AGB estimation, which, however, cannot directly provide information on vegetation structure or non-optical characteristics [18,110]. Moreover, compared with natural ecosystems, urban vegetation exhibits fine-scale heterogeneous distribution patterns, and building shadows interfere with spectral signals, causing distortion in the Normalized Difference Vegetation Index (NDVI) and leading to error rates of 30–50% in traditional optical remote sensing models [111]. Future research should integrate multi-source data and incorporate non-optical remote sensing indicators to construct a multi-dimensional urban AGB inversion database, aiming to enhance the simulation of vegetation physiological processes.

5. Conclusions

The precise estimation of urban trees' AGB is crucial for evaluating regional carbon budgets and maintaining ecosystem balance. Focusing on 51 C40 cities in Eurasia continent, this study applied quality control strategies to optimize a RF model, enabling high-resolution, large-scale inversion of urban trees' AGB. On this basis, AGB density and total AGB were further calculated, and the estimates were compared with existing study data. In terms of model performance, this study fully leveraged multi-source remote sensing data and applied stringent quality control to select highly reliable samples. Ten-fold cross validation yielded a mean R^2 increase from 0.37 to 0.75 and a reduction in MAE from 47.02 Mg/ha to 17.48 Mg/ha, substantially improving both model fit and predictive accuracy. For AGB accounting, the average AGB density of C40 cities in Eurasian is 39.44 Mg/ha, with a total AGB of 83.83 $\times$$10^6$ t. In terms of AGB density, East and Southeast Asia show the highest regional average at 43.81 Mg/ha, whereas those in South and West

Asia exhibit the lowest at 31.98 Mg/ha. As for total AGB, the East and Southeast Asia (8.87 $\times 10^6$ t) and South and West Asia (5.23 $\times 10^6$ t) fall below the regional mean, whereas the Central East Asia records the highest total at 48.70 $\times 10^6$ t. Furthermore, comparative analyses with existing single-city C40 studies, the errors in AGB, and AGB density in this study remain within acceptable bounds. Based on existing AGB data products, this study developed a systematic data preprocessing and accounting framework, enabling 10 m–resolution high-precision mapping of urban trees' AGB. Collectively, the proposed framework in this study can be confidently applied for large-scale, fine-resolution AGB mapping of urban trees' AGB across heterogeneous urban environments, supporting regional carbon accounting, urban forestry planning, and urban ecosystem function evaluation.

Supplementary Materials: The following supporting information can be downloaded at: https://www.mdpi.com/article/10.3390/rs17233898/s1, Table S1: Major Köppen-Geiger climatic types with representative C40 Cities; Table S2: Sentinel-2 raw image data used for each city; Table S3: Configuration of random forest model hyperparameters; Table S4: Vegetation indices and calculation formulas used in this study; Table S5: Texture features and their calculation formulas used in this study; Table S6: Feature variables were selected from muti-source data; Method S1: Urban Trees Outside Forests (TOF) data extraction; Method S2: 10-m Canopy Height Data Construction; Figure S1: Differences in the representation of urban TOF features by canopy height data at different resolutions; (a) low resolution; (b) high resolution.

Author Contributions: Conceptualization, K.C., N.L., G.L. and G.Y.; methodology and formal analysis, G.Y., Z.S., G.L., M.C. and Y.C.; data curation, K.C., N.L., Y.L. and S.Z.; writing—original draft preparation, G.Y., Z.S., M.C. and Y.C.; writing—review and editing, Y.C. and M.C. All authors have read and agreed to the published version of the manuscript.

Funding: This study is supported by the National Natural Science Foundation of China (42071415 and 42501143), Postgraduate Quality Teaching Materials Project of Henan Province (YIS2023JC22), Ministry of Education Industry-University Cooperation and Collaborative Education Project, Practice Base Construction Project (230902313171729), University Science and Technology Innovation Team in Henan Province (25IRTSTHN004), Central Plains Youth Top Talent Project, and Xinyang Academy of Ecological Research Open Foundation (2023XYMS01), Natural Science Foundation of Henan (252300420827).

Data Availability Statement: The original contributions presented in the study are included in the article; further inquiries can be directed to the corresponding author.

Conflicts of Interest: The authors declare that they have no known competing financial interests or personal relationships that could have appeared to influence the work reported in this paper.

References

1. Diezmartínez, C.V.; Sovacool, B.K.; Short Gianotti, A.G. Operationalizing climate justice in the implementation of Boston's Building Performance Standard. *Nat. Cities* **2024**, *1*, 665–676. [CrossRef]
2. Sun, Y.-L.; Zhang, C.-H.; Lian, Y.-J.; Zhao, J.-M. Exploring the Global Research Trends of Cities and Climate Change Based on a Bibliometric Analysis. *Sustainability* **2022**, *14*, 12302. [CrossRef]
3. Davidson, K.; Coenen, L.; Gleeson, B. A decade of C40: Research insights and agendas for city networks. *Glob. Policy* **2019**, *10*, 697–708. [CrossRef]
4. Román, M. Governing from the middle: The C40 Cities Leadership Group. *Corp. Gov. Int. J. Bus. Soc.* **2010**, *10*, 73–84.
5. Cui, K.; Cui, Y.; Deng, X.; Zhang, C.; Jia, Y.; Zhao, T.; Li, N.; Shi, Z.; Zhao, X.; Qin, H. Refined big data on carbon sequestration for urban trees: 3D information and spatial carbon stock. *Sustain. Cities Soc.* **2025**, *134*, 106901. [CrossRef]
6. Johnson, L.; Krisko, P.; Malik, M.; O'Donnell, C.; Pendleton, N.; Ahn, D.; Bizberg, A.; Chafe, Z.A.; Kim, D.; McCormick, S. Environmental, health, and equity co-benefits in urban climate action plans: A descriptive analysis for 27 C40 member cities. *Front. Sustain. Cities* **2022**, *4*, 869203. [CrossRef]
7. Liu, X.; Cui, Y.; Xiao, X.; Shi, Z.; Li, M.; Li, N.; Dong, J. Multi-scale analysis of urbanization and gross primary productivity during 2000–2018 in Beijing, China. *Environ. Res. Lett.* **2023**, *19*, 014023. [CrossRef]

8. Agbelade, A.D.; Onyekwelu, J.C. Tree species diversity, volume yield, biomass and carbon sequestration in urban forests in two Nigerian cities. *Urban Ecosyst.* **2020**, *23*, 957–970. [CrossRef]
9. Li, N.; Deng, L.; Yan, G.; Cao, M.; Cui, Y. Estimation for refined carbon storage of urban green space and minimum spatial mapping scale in a plain city of China. *Remote Sens.* **2024**, *16*, 217. [CrossRef]
10. Kükenbrink, D.; Gardi, O.; Morsdorf, F.; Thürig, E.; Schellenberger, A.; Mathys, L. Above-ground biomass references for urban trees from terrestrial laser scanning data. *Ann. Bot.* **2021**, *128*, 709–724. [CrossRef] [PubMed]
11. Tian, L.; Wu, X.; Tao, Y.; Li, M.; Qian, C.; Liao, L.; Fu, W. Review of remote sensing-based methods for forest aboveground biomass estimation: Progress, challenges, and prospects. *Forests* **2023**, *14*, 1086. [CrossRef]
12. Wilkes, P.; Disney, M.; Vicari, M.B.; Calders, K.; Burt, A. Estimating urban above ground biomass with multi-scale LiDAR. *Carbon Balance Manag.* **2018**, *13*, 10. [CrossRef]
13. Hojas Gascon, L.; Ceccherini, G.; Garcia Haro, F.J.; Avitabile, V.; Eva, H. The potential of high resolution (5 m) RapidEye optical data to estimate above ground biomass at the national level over Tanzania. *Forests* **2019**, *10*, 107. [CrossRef]
14. Rijal, S.S.; Pham, T.D.; Noer'Aulia, S.; Putera, M.I.; Saintilan, N. Mapping mangrove above-ground carbon using multi-source remote sensing data and machine learning approach in Loh Buaya, Komodo National Park, Indonesia. *Forests* **2023**, *14*, 94. [CrossRef]
15. Tigges, J.; Lakes, T. High resolution remote sensing for reducing uncertainties in urban forest carbon offset life cycle assessments. *Carbon Balance Manag.* **2017**, *12*, 17. [CrossRef]
16. Sharma, G.; Morgenroth, J.; Richards, D.R.; Ye, N. Advancing urban forest and ecosystem service assessment through the integration of remote sensing and i-Tree Eco: A systematic review. *Urban For. Urban Green.* **2025**, *104*, 128659. [CrossRef]
17. Kowe, P.; Mutanga, O.; Dube, T. Advancements in the remote sensing of landscape pattern of urban green spaces and vegetation fragmentation. *Int. J. Remote Sens.* **2021**, *42*, 3797–3832. [CrossRef]
18. Ahmad, A.; Gilani, H.; Ahmad, S.R. Forest aboveground biomass estimation and mapping through high-resolution optical satellite imagery—A literature review. *Forests* **2021**, *12*, 914. [CrossRef]
19. Ma, P.; Lin, H.; Wang, W.; Yu, H.; Chen, F.; Jiang, L.; Zhou, L.; Zhang, Z.; Shi, G.; Wang, J. Toward fine surveillance: A review of multitemporal interferometric synthetic aperture radar for infrastructure health monitoring. *IEEE Geosci. Remote Sens. Mag.* **2021**, *10*, 207–230. [CrossRef]
20. Guo, Q.; Su, Y.; Hu, T.; Guan, H.; Jin, S.; Zhang, J.; Zhao, X.; Xu, K.; Wei, D.; Kelly, M. Lidar boosts 3D ecological observations and modelings: A review and perspective. *IEEE Geosci. Remote Sens. Mag.* **2020**, *9*, 232–257. [CrossRef]
21. Zhang, S.; Li, N.; Cui, Y.; Dong, J.; Yu, L.; Ran, L.; Chen, Z.; Niu, J.; Yan, W.; Kanniah, K.D.; et al. Large-Scale Single Tree Information Extraction of Oil Palm in Malaysia Based on Sub-Meter Visible Light Satellite Images. *Comput. Electron. Agric.* **2025**, *238*, 110796. [CrossRef]
22. Zhang, Y.; Shao, Z. Assessing of urban vegetation biomass in combination with LiDAR and high-resolution remote sensing images. *Int. J. Remote Sens.* **2021**, *42*, 964–985. [CrossRef]
23. Yang, M.; Zhou, X.; Liu, Z.; Li, P.; Tang, J.; Xie, B.; Peng, C. A review of general methods for quantifying and estimating urban trees and biomass. *Forests* **2022**, *13*, 616. [CrossRef]
24. Araza, A.; Herold, M.; De Bruin, S.; Ciais, P.; Gibbs, D.A.; Harris, N.; Santoro, M.; Wigneron, J.-P.; Yang, H.; Málaga, N. Past decade above-ground biomass change comparisons from four multi-temporal global maps. *Int. J. Appl. Earth Obs. Geoinf.* **2023**, *118*, 103274. [CrossRef]
25. Safari, A.; Sohrabi, H.; Powell, S. Comparison of satellite-based estimates of aboveground biomass in coppice oak forests using parametric, semiparametric, and nonparametric modeling methods. *J. Appl. Remote Sens.* **2018**, *12*, 046026. [CrossRef]
26. Chirici, G.; Barbati, A.; Corona, P.; Marchetti, M.; Travaglini, D.; Maselli, F.; Bertini, R. Non-parametric and parametric methods using satellite images for estimating growing stock volume in alpine and Mediterranean forest ecosystems. *Remote Sens. Environ.* **2008**, *112*, 2686–2700. [CrossRef]
27. Urbazaev, M.; Thiel, C.; Cremer, F.; Dubayah, R.; Migliavacca, M.; Reichstein, M.; Schmullius, C. Estimation of forest aboveground biomass and uncertainties by integration of field measurements, airborne LiDAR, and SAR and optical satellite data in Mexico. *Carbon Balance Manag.* **2018**, *13*, 5. [CrossRef] [PubMed]
28. Su, H.; Shen, W.; Wang, J.; Ali, A.; Li, M. Machine learning and geostatistical approaches for estimating aboveground biomass in Chinese subtropical forests. *For. Ecosyst.* **2020**, *7*, 64. [CrossRef]
29. Wu, C.; Tao, H.; Zhai, M.; Lin, Y.; Wang, K.; Deng, J.; Shen, A.; Gan, M.; Li, J.; Yang, H. Using nonparametric modeling approaches and remote sensing imagery to estimate ecological welfare forest biomass. *J. For. Res.* **2018**, *29*, 151–161. [CrossRef]
30. Ma, T.; Zhang, C.; Ji, L.; Zuo, Z.; Beckline, M.; Hu, Y.; Li, X.; Xiao, X. Development of forest aboveground biomass estimation, its problems and future solutions: A review. *Ecol. Indic.* **2024**, *159*, 111653. [CrossRef]
31. Li, Z.; Bi, S.; Hao, S.; Cui, Y. Aboveground biomass estimation in forests with random forest and Monte Carlo-based uncertainty analysis. *Ecol. Indic.* **2022**, *142*, 109246. [CrossRef]

32. Dorado-Roda, I.; Pascual, A.; Godinho, S.; Silva, C.A.; Botequim, B.; Rodríguez-Gonzálvez, P.; González-Ferreiro, E.; Guerra-Hernández, J. Assessing the accuracy of GEDI data for canopy height and aboveground biomass estimates in Mediterranean forests. *Remote Sens.* **2021**, *13*, 2279. [CrossRef]
33. Sialelli, G.; Peters, T.; Wegner, J.D.; Schindler, K. Agbd: A global-scale biomass dataset. *arXiv* **2024**, arXiv:2406.04928 2024. [CrossRef]
34. Heikkinen, M.; Ylä-Anttila, T.; Juhola, S. Incremental, reformistic or transformational: What kind of change do C40 cities advocate to deal with climate change? *J. Environ. Policy Plan.* **2019**, *21*, 90–103. [CrossRef]
35. Lasantha, V.; Oki, T.; Tokuda, D. Data–Driven versus Köppen–Geiger Systems of Climate Classification. *Adv. Meteorol.* **2022**, *2022*, 3581299. [CrossRef]
36. Martin, G.K.; O'Dell, K.; Kinney, P.; Pescador-Jimenez, M.; Rojas-Rueda, D.; Canales, R.; Anenberg, S. Tracking progress towards urban nature targets using landcover and vegetation indices: A global study for the 96 C40 Cities. *GeoHealth* **2024**, *8*, 3. [CrossRef]
37. Quegan, S.; Le Toan, T.; Chave, J.; Dall, J.; Exbrayat, J.-F.; Minh, D.H.T.; Lomas, M.; D'alessandro, M.M.; Paillou, P.; Papathanassiou, K. The European Space Agency BIOMASS mission: Measuring forest above-ground biomass from space. *Remote Sens. Environ.* **2019**, *227*, 44–60. [CrossRef]
38. Zhou, Y.; Taylor, D.M.; Tang, H. Improved country-wide estimation of above-ground tropical forest biomass using locally calibrated GEDI spaceborne LiDAR data. *Environ. Res. Lett.* **2024**, *20*, 014017. [CrossRef]
39. Venter, Z.S.; Barton, D.N.; Chakraborty, T.; Simensen, T.; Singh, G. Global 10 m land use land cover datasets: A comparison of dynamic world, world cover and esri land cover. *Remote Sens.* **2022**, *14*, 4101. [CrossRef]
40. da Silva, W.K.K.; Dudeque Zenni, R.; de Carvalho Alves, M. Urbanization Increases Gross Primary Production and Biomass of Atlantic Forest Fragments. *Acta Oecologica* **2025**, *129*, 104126. [CrossRef]
41. Breiman, L. Statistical modeling: The two cultures (with comments and a rejoinder by the author). *Stat. Sci.* **2001**, *16*, 199–231. [CrossRef]
42. Rigatti, S.J. Random forest. *J. Insur. Med.* **2017**, *47*, 31–39. [CrossRef] [PubMed]
43. Hengl, T.; Heuvelink, G.B.; Kempen, B.; Leenaars, J.G.; Walsh, M.G.; Shepherd, K.D.; Sila, A.; MacMillan, R.A.; Mendes de Jesus, J.; Tamene, L. Mapping soil properties of Africa at 250 m resolution: Random forests significantly improve current predictions. *PLoS ONE* **2015**, *10*, e0125814. [CrossRef]
44. Xu, W.; Cheng, Y.; Luo, M.; Mai, X.; Wang, W.; Zhang, W.; Wang, Y. Progress and Limitations in Forest Carbon Stock Estimation Using Remote Sensing Technologies: A Comprehensive Review. *Forests* **2025**, *16*, 449. [CrossRef]
45. Wood, E.M.; Pidgeon, A.M.; Radeloff, V.C.; Keuler, N.S. Image texture as a remotely sensed measure of vegetation structure. *Remote Sens. Environ.* **2012**, *121*, 516–526. [CrossRef]
46. Xue, J.; Su, B. Significant remote sensing vegetation indices: A review of developments and applications. *J. Sens.* **2017**, *2017*, 1353691. [CrossRef]
47. Dong, T.; Meng, J.; Shang, J.; Liu, J.; Wu, B.; Huffman, T. Modified vegetation indices for estimating crop fraction of absorbed photosynthetically active radiation. *Int. J. Remote Sens.* **2015**, *36*, 3097–3113. [CrossRef]
48. Matsushita, B.; Yang, W.; Chen, J.; Onda, Y.; Qiu, G. Sensitivity of the enhanced vegetation index (EVI) and normalized difference vegetation index (NDVI) to topographic effects: A case study in high-density cypress forest. *Sensors* **2007**, *7*, 2636–2651. [CrossRef]
49. Nandy, S.; Srinet, R.; Padalia, H. Mapping forest height and aboveground biomass by integrating ICESat–2, Sentinel–1 and Sentinel–2 data using Random Forest algorithm in northwest Himalayan foothills of India. *Geophys. Res. Lett.* **2021**, *48*, e2021GL093799. [CrossRef]
50. Huete, A.; Didan, K.; Miura, T.; Rodriguez, E.P.; Gao, X.; Ferreira, L.G. Overview of the radiometric and biophysical performance of the MODIS vegetation indices. *Remote Sens. Environ.* **2002**, *83*, 195–213. [CrossRef]
51. Nadjla, B.; Assia, S.; Ahmed, Z. Contribution of spectral indices of chlorophyll (RECl and GCI) in the analysis of multi-temporal mutations of cultivated land in the Mostaganem plateau. In Proceedings of the 2022 7th International Conference on Image and Signal Processing and Their Applications (ISPA), Mostaganem, Algeria, 8–9 May 2022; pp. 1–6.
52. Lemenkova, P.; Debeir, O. Computing vegetation indices from the satellite images using GRASS GIS scripts for monitoring mangrove forests in the coastal landscapes of Niger Delta, Nigeria. *J. Mar. Sci. Eng.* **2023**, *11*, 871. [CrossRef]
53. Stow, D.; Niphadkar, M.; Kaiser, J. MODIS-derived visible atmospherically resistant index for monitoring chaparral moisture content. *Int. J. Remote Sens.* **2005**, *26*, 3867–3873. [CrossRef]
54. Kimura, R.; Okada, S.; Miura, H.; Kamichika, M. Relationships among the leaf area index, moisture availability, and spectral reflectance in an upland rice field. *Agric. Water Manag.* **2004**, *69*, 83–100. [CrossRef]
55. Wilson, N.R.; Norman, L.M. Analysis of vegetation recovery surrounding a restored wetland using the normalized difference infrared index (NDII) and normalized difference vegetation index (NDVI). *Int. J. Remote Sens.* **2018**, *39*, 3243–3274. [CrossRef]
56. Yue, J.; Yao, Y.; Shen, J.; Li, T.; Xu, N.; Feng, H.; Wei, Y.; Xu, X.; Lin, Y.; Guo, W. Winter wheat harvest detection via Sentinel-2 MSI images. *Int. J. Remote Sens.* **2025**, *46*, 2482–2500. [CrossRef]
57. Bannari, A.; Morin, D.; Bonn, F.; Huete, A. A review of vegetation indices. *Remote Sens. Rev.* **1995**, *13*, 95–120. [CrossRef]

58. Liu, M.; Zhan, Y.; Li, J.; Kang, Y.; Sun, X.; Gu, X.; Wei, X.; Wang, C.; Li, L.; Gao, H. Validation of red-edge vegetation indices in vegetation classification in tropical monsoon region—A case study in Wenchang, Hainan, China. *Remote Sens.* **2024**, *16*, 1865. [CrossRef]
59. Zhang, H.; Li, J.; Liu, Q.; Lin, S.; Huete, A.; Liu, L.; Croft, H.; Clevers, J.G.; Zeng, Y.; Wang, X. A novel red-edge spectral index for retrieving the leaf chlorophyll content. *Methods Ecol. Evol.* **2022**, *13*, 2771–2787. [CrossRef]
60. Magney, T.S.; Eitel, J.U.; Vierling, L.A. Mapping wheat nitrogen uptake from RapidEye vegetation indices. *Precis. Agric.* **2017**, *18*, 429–451. [CrossRef]
61. Sharifi, A. Using sentinel-2 data to predict nitrogen uptake in maize crop. *IEEE J. Sel. Top. Appl. Earth Obs. Remote Sens. Environ.* **2020**, *13*, 2656–2662. [CrossRef]
62. Gitelson, A.A.; Kaufman, Y.J.; Merzlyak, M.N. Use of a green channel in remote sensing of global vegetation from EOS-MODIS. *Remote Sens. Environ.* **1996**, *58*, 289–298. [CrossRef]
63. Wu, W. The generalized difference vegetation index (GDVI) for dryland characterization. *Remote Sens.* **2014**, *6*, 1211–1233. [CrossRef]
64. Frampton, W.J.; Dash, J.; Watmough, G.; Milton, E.J. Evaluating the capabilities of Sentinel-2 for quantitative estimation of biophysical variables in vegetation. *ISPRS J. Photogramm. Remote Sens.* **2013**, *82*, 83–92. [CrossRef]
65. Majasalmi, T.; Rautiainen, M. The potential of Sentinel-2 data for estimating biophysical variables in a boreal forest: A simulation study. *Remote Sens. Lett.* **2016**, *7*, 427–436. [CrossRef]
66. Dong, T.; Meng, J.; Shang, J.; Liu, J.; Wu, B. Evaluation of chlorophyll-related vegetation indices using simulated Sentinel-2 data for estimation of crop fraction of absorbed photosynthetically active radiation. *IEEE J. Sel. Top. Appl. Earth Obs. Remote Sens.* **2015**, *8*, 4049–4059. [CrossRef]
67. Guan, Q.; Huang, W.; Zhao, J.; Liu, L.; Liang, D.; Huang, L.; Wang, L.; Yang, G. Quantitative identification of yellow rust, powdery mildew and fertilizer-water stress in winter wheat using in-situ hyperspectral data. *Sens. Lett.* **2014**, *12*, 876–882. [CrossRef]
68. Xu, D.; Zhang, M. Mapping paddy rice using an adaptive stacking algorithm and Sentinel-1/2 images based on Google Earth Engine. *Remote Sens. Lett.* **2022**, *13*, 373–382. [CrossRef]
69. Xie, Q.; Dash, J.; Huang, W.; Peng, D.; Qin, Q.; Mortimer, H.; Casa, R.; Pignatti, S.; Laneve, G.; Pascucci, S. Vegetation indices combining the red and red-edge spectral information for leaf area index retrieval. *IEEE J. Sel. Top. Appl. Earth Obs. Remote Sens.* **2018**, *11*, 1482–1493. [CrossRef]
70. Fernández-Manso, A.; Fernández-Manso, O.; Quintano, C. SENTINEL-2A red-edge spectral indices suitability for discriminating burn severity. *nt. J. Appl. Earth Obs. Geoinf.* **2016**, *50*, 170–175. [CrossRef]
71. Radočaj, D.; Šiljeg, A.; Marinović, R.; Jurišić, M. State of major vegetation indices in precision agriculture studies indexed in web of science: A review. *Agriculture* **2023**, *13*, 707. [CrossRef]
72. Feng, W.; Wu, Y.; He, L.; Ren, X.; Wang, Y.; Hou, G.; Wang, Y.; Liu, W.; Guo, T. An optimized non-linear vegetation index for estimating leaf area index in winter wheat. *Precis. Agric.* **2019**, *20*, 1157–1176. [CrossRef]
73. Ren, S.; Chen, X.; An, S. Assessing plant senescence reflectance index-retrieved vegetation phenology and its spatiotemporal response to climate change in the Inner Mongolian Grassland. *Int. J. Biometeorol.* **2017**, *61*, 601–612. [CrossRef] [PubMed]
74. Rondeaux, G.; Steven, M.; Baret, F. Optimization of soil-adjusted vegetation indices. *Remote Sens. Environ.* **1996**, *55*, 95–107. [CrossRef]
75. Gitelson, A.A. Wide dynamic range vegetation index for remote quantification of biophysical characteristics of vegetation. *J. Plant Physiol.* **2004**, *161*, 165–173. [CrossRef] [PubMed]
76. Schiefer, F.; Schmidtlein, S.; Frick, A.; Frey, J.; Klinke, R.; Zielewska-Büttner, K.; Junttila, S.; Uhl, A.; Kattenborn, T. UAV-based reference data for the prediction of fractional cover of standing deadwood from Sentinel time series. *ISPRS Open J. Photogramm. Remote Sens.* **2023**, *8*, 100034. [CrossRef]
77. Mavrogiorgos, K.; Kiourtis, A.; Mavrogiorgou, A.; Menychtas, A.; Kyriazis, D. Bias in machine learning: A literature review. *Appl. Sci.* **2024**, *14*, 8860. [CrossRef]
78. Lamahewage, S.H.G.; Witharana, C.; Riemann, R.; Fahey, R.; Worthley, T. Comparing Machine Learning and Statistical Models for Remote Sensing-Based Forest Aboveground Biomass Estimations. *Forests* **2025**, *16*, 1430. [CrossRef]
79. Huang, D.; Zhou, Z.; Zhang, Z.; Dai, Q.; Lu, H.; Li, Y.; Huang, Y. Land Use/Land Cover Remote Sensing Classification in Complex Subtropical Karst Environments: Challenges, Methodological Review, and Research Frontiers. *Appl. Sci.* **2025**, *15*, 9641. [CrossRef]
80. Zakaria, Y.S.; Akhir, M.F.; Muslim, A.M.; Ariffin, N.A.; Ahmad, A. Estimating Forest Aboveground Biomass Density Using Remote Sensing and Machine Learning: A RSME Approach. *Land Degrad. Dev.* **2025**. [CrossRef]
81. Li, Y.; Li, M.; Wang, Y. Forest aboveground biomass estimation and response to climate change based on remote sensing data. *Sustainability* **2022**, *14*, 14222. [CrossRef]
82. Li, J.; Bao, W.; Wang, X.; Song, Y.; Liao, T.; Xu, X.; Guo, M. Estimating Aboveground Biomass of Boreal forests in Northern China using multiple datasets. *IEEE Trans. Geosci. Remote Sens.* **2024**, *62*, 1–10. [CrossRef]

83. Wong, T.-T.; Yeh, P.-Y. Reliable accuracy estimates from k-fold cross validation. *IEEE Trans. Knowl. Data Eng.* **2019**, *32*, 1586–1594. [CrossRef]
84. Li, W.; Cui, Y.; Liu, X.; Deng, C.; Zhang, S. Positive impact of urbanization on vegetation growth has been continuously strengthening in arid regions of China. *Environ. Res. Lett.* **2023**, *18*, 124011. [CrossRef]
85. Woodward, A.; Hinwood, A.; Bennett, D.; Grear, B.; Vardoulakis, S.; Lalchandani, N.; Lyne, K.; Williams, C. Trees, climate change, and health: An urban planning, greening and implementation perspective. *Int. J. Environ. Res. Public Health* **2023**, *20*, 6798. [CrossRef] [PubMed]
86. Zhu, Y.; Feng, Z.; Lu, J.; Liu, J. Estimation of forest biomass in Beijing (China) using multisource remote sensing and forest inventory data. *Forests* **2020**, *11*, 163. [CrossRef]
87. Zhang, Y.; Li, X. Carbon sink potential of Beijing's forest under carbon peak and cabon neutrality. *Resour. Ind.* **2022**, *24*, 15.
88. Ren, D.; Liao, X.; Xiao, Q.; Lai, C.; Song, F.; Meng, S.; Peng, X. Carbon storage and spatial distribution pattern of forest vegetation in Chengdu. *J. West China For. Sci.* **2021**, *50*, 74–81.
89. Mariappan, M.; Lingava, S.; Murugaiyan, R.; Krishnan, V.; Kolanuvada, S.R.; Thirumeni, R.S.L. Carbon accounting of urban forest in Chennai City using Lidar data. *Eur. J. Sci. Res.* **2012**, *81*, 314–328.
90. Wang, Z.; Liu, H.; Guan, Q.; Wang, X.; Hao, J.; Ling, N.; Shi, C. Carbon storage and density of urban forest ecosystems in Nanjing. *J. Nanjing For. Univ. (Nat. Sci. Ed.)* **2011**, *35*, 18–22.
91. Fan, D.; Yu, X.; Yue, Y.; Niu, L.; Gao, Z.; Ma, L. Forest carbon storage and its dynamics in Beijing. *J. Beijing For. Univ.* **2008**, *30*, 117–120.
92. Chen, Y.; Shi, Z.; Zeng, W.; Yuan, F.; Wang, Y.; Zeng, C. Estimation and Distribution Characteristics of Carbon Density in the Arbor Layer of Urban Green Spaces in Shenzhen's Built Area. *J. Chin. Urban For.* **2024**, *22*, 43–50.
93. Tan, Y.; Peng, Y.; Shi, Z.; Wen, W. Forest Carbon Storage and Its Dynamic Change in Shenzhen City. *J. Southwest For. Univ. (Nat. Sci.)* **2013**, *33*, 17–24.
94. Richter, S.; Haase, D.; Thestorf, K.; Makki, M. Carbon pools of berlin, germany: Organic carbon in soils and aboveground in trees. *Urban For. Urban Green.* **2020**, *54*, 126777. [CrossRef]
95. Wei, F.; Zhan, X. Delineation of rigid urban growth boundary based on habitat quality and carbon storage. *J. Zhejiang Univ. (Eng. Sci.)* **2019**, *53*, 1478–1487.
96. Schwartz, M.; Ciais, P.; De Truchis, A.; Chave, J.; Ottlé, C.; Vega, C.; Wigneron, J.-P.; Nicolas, M.; Jouaber, S.; Liu, S. FORMS: Forest Multiple Source height, wood volume, and biomass maps in France at 10 to 30 m resolution based on Sentinel-1, Sentinel-2, and Global Ecosystem Dynamics Investigation (GEDI) data with a deep learning approach. *Earth Syst. Sci. Data* **2023**, *15*, 4927–4945. [CrossRef]
97. Davies, Z.G.; Dallimer, M.; Edmondson, J.L.; Leake, J.R.; Gaston, K.J. Identifying potential sources of variability between vegetation carbon storage estimates for urban areas. *Environ. Pollut.* **2013**, *183*, 133–142. [CrossRef] [PubMed]
98. Xu, F.; Liu, W.; Ren, W.; Zhong, Q.; Zhang, G.; Wang, K. Effects of community structure on carbon fixation of urban forests in Shanghai, China. *Chin. J. Ecol.* **2010**, *29*, 439–447.
99. Velasco, E.; Chen, K.W. Carbon storage estimation of tropical urban trees by an improved allometric model for aboveground biomass based on terrestrial laser scanning. *Urban For. Urban Green.* **2019**, *44*, 126387. [CrossRef]
100. Liu, S.; Brandt, M.; Nord-Larsen, T.; Chave, J.; Reiner, F.; Lang, N.; Tong, X.; Ciais, P.; Igel, C.; Pascual, A. The overlooked contribution of trees outside forests to tree cover and woody biomass across Europe. *Sci. Adv.* **2023**, *9*, eadh4097. [CrossRef]
101. Miettinen, J.; Breidenbach, J.; Adame, P.; Adolt, R.; Alberdi, I.; Antropov, O.; Arnarsson, Ó.; Astrup, R.; Berger, A.; Bogason, J. Pan-European forest maps produced with a combination of earth observation data and national forest inventory plots. *Data Brief* **2025**, *60*, 111613. [CrossRef]
102. Shendryk, Y. Fusing GEDI with earth observation data for large area aboveground biomass mapping. *Int. J. Appl. Earth Obs. Geoinf.* **2022**, *115*, 103108. [CrossRef]
103. Santoro, M.; Cartus, O. ESA Biomass Climate Change Initiative (Biomass_cci): Global Datasets of Forest Above-Ground Biomass for the Years 2010, 2017 and 2018, v3. NERC EDS Centre for Environmental Data Analysis. 2021. Available online: https://catalogue.ceda.ac.uk/uuid/5f331c418e9f4935b8eb1b836f8a91b8/ (accessed on 2 October 2024).
104. Santoro, M.; Cartus, O. ESA Biomass Climate Change Initiative (Biomass_cci): Global Datasets of Forest Above-Ground Biomass for the Years 2010, 2017, 2018, 2019 and 2020, v4. NERC EDS Centre for Environmental Data Analysis. 2023. Available online: https://catalogue.ceda.ac.uk/uuid/af60720c1e404a9e9d2c145d2b2ead4e/ (accessed on 2 October 2024).
105. Hunka, N.; Duncanson, L.; Armston, J.; Dubayah, R.; Healey, S.P.; Santoro, M.; May, P.; Araza, A.; Bourgoin, C.; Montesano, P.M. Intergovernmental panel on climate change (IPCC) tier 1 forest biomass estimates from Earth observation. *Sci. Data* **2024**, *11*, 1127. [CrossRef]
106. Pasher, J.; McGovern, M.; Khoury, M.; Duffe, J. Assessing carbon storage and sequestration by Canada's urban forests using high resolution earth observation data. *Urban For. Urban Green.* **2014**, *13*, 484–494. [CrossRef]

107. Santoro, M.; Cartus, O.; Carvalhais, N.; Rozendaal, D.M.; Avitabile, V.; Araza, A.; De Bruin, S.; Herold, M.; Quegan, S.; Rodríguez-Veiga, P. The global forest above-ground biomass pool for 2010 estimated from high-resolution satellite observations. *Earth Syst. Sci. Data* **2021**, *13*, 3927–3950. [CrossRef]
108. Davies, Z.G.; Edmondson, J.L.; Heinemeyer, A.; Leake, J.R.; Gaston, K.J. Mapping an urban ecosystem service: Quantifying above–ground carbon storage at a city–wide scale. *J. Appl. Ecol.* **2011**, *48*, 1125–1134. [CrossRef]
109. Liu, X.; Wang, S.; Wu, P.; Feng, K.; Hubacek, K.; Li, X.; Sun, L. Impacts of urban expansion on terrestrial carbon storage in China. *Environ. Sci. Technol.* **2019**, *53*, 6834–6844. [CrossRef]
110. Lu, D.; Chen, Q.; Wang, G.; Liu, L.; Li, G.; Moran, E. A survey of remote sensing-based aboveground biomass estimation methods in forest ecosystems. *Int. J. Digit. Earth* **2016**, *9*, 63–105. [CrossRef]
111. Myneni, R.; Maggion, S.; Iaquinta, J.; Privette, J.; Gobron, N.; Pinty, B.; Kimes, D.; Verstraete, M.; Williams, D. Optical remote sensing of vegetation: Modeling, caveats, and algorithms. *Remote Sens. Environ.* **1995**, *51*, 169–188. [CrossRef]

Disclaimer/Publisher's Note: The statements, opinions and data contained in all publications are solely those of the individual author(s) and contributor(s) and not of MDPI and/or the editor(s). MDPI and/or the editor(s) disclaim responsibility for any injury to people or property resulting from any ideas, methods, instructions or products referred to in the content.